Research Article | Vol. 31, No. 22 / 23 Oct 2023 / Optics Express 36590
Optics EXPRESS

Multi-parameter distributed fiber optic sensing using double-Brillouin peak fiber in Brillouin optical time domain analysis

NAGESWARA LALAM,[1,2,7] HARI BHATTA,[1,3] XIAOGUANG SUN,[4] PING LU,[4] PAUL OHODNICKI,[5] MICHAEL P. BURIC,[6] AND RUISHU WRIGHT[1,8]

[1]National Energy Technology Laboratory, 626 Cochran Mill Road, Pittsburgh, PA 15236, USA
[2]NETL Support Contractor, 626 Cochran Mill Road, Pittsburgh, PA 15236, USA
[3]Oak Ridge Institute for Science and Education (ORISE), 1299 Bethel Valley Rd., Oak Ridge, TN, USA
[4]OFS Fitel, LLC, 55 Darling Dr., Avon, CT 06001, USA
[5]Mechanical Engineering & Materials Science, University of Pittsburgh, Pittsburgh, PA 15261, USA
[6]National Energy Technology Laboratory, 3610 Collins Ferry Road, Morgantown, WV 26505, USA
[7]nageswara.lalam@netl.doe.gov
[8]ruishu.wright@netl.doe.gov

Abstract: In this paper, we demonstrate a multi-parameter fiber sensing system based on stimulated Brillouin scattering in a double-Brillouin peak specialty fiber with enhanced Brillouin gain response. The amplitude level of the second Brillouin gain peak, which originated from the higher-order acoustic modes, has been improved with an approximately similar amplitude level to the first Brillouin gain peak from the fundamental acoustic mode. Compared to other multi-Brillouin peak fibers presented in the literature, the proposed fiber significantly reduces the measured Brillouin frequency shift error, thus improving strain and temperature accuracies. By utilizing the sensitivity values of the strain and temperature associated with each Brillouin gain spectrum (BGS) peak, a successful discriminative measurement of strain and temperature is performed with an accuracy of ±13 με, and ±0.5 °C, respectively. The proposed double-Brillouin peak fiber appears to be a possible alternative to other multi-BGS peak fibers, for instance, large effective area fiber and dispersion compensating fibers, which are inherently accompanied by large measurement errors due to the weak Brillouin gain values originating from the higher-order acoustic modes. The demonstrated results show different strain and temperature coefficients of 47 kHz/με, 1.15 MHz/°C for peak 1 and 51 kHz/με, 1.37 MHz/°C for peak 2. Moreover, the enhanced BGS peak gains having nearly the same amplitude levels enable the discriminative measurement of strain and temperature. Such fibers in Brillouin interrogation eliminate the need for complex monitoring setups and reduce measurement errors. We recommend that for long-distance natural gas pipeline monitoring, where discriminative strain and temperature measurement is crucial, the proposed double-Brillouin peak fiber can be highly beneficial.

1. Introduction

Fiber optic sensors have unique advantages over conventional sensors, including high sensitivity, immunity to electromagnetic interference, multiplexing or distributed sensing capabilities, resistance to harsh environments, lightweight, easily attachable/ embeddable to any type of material, and the ability to transmit signals over long distances [1]. There has been a continuous trend and necessity to sense more physical parameters to better control infrastructural safety, spur economic growth, and provide real-time and reliable sensing data, usually through distributed fiber optic sensing technology. Over the past few decades, Brillouin-based distributed fiber optic sensors have gained attention due to their long-distance strain and/or temperature monitoring

#498141 https://doi.org/10.1364/OE.498141
Journal © 2023 Received 27 Jun 2023; revised 25 Aug 2023; accepted 28 Sep 2023; published 17 Oct 2023

Optics EXPRESS

capability over tens of kilometers at high spatial resolutions in the range of a meter or even centimeters [2,3]. One major advantage of these types of sensors is their ability to have early spatial information on possible failures/damages within the infrastructure, thereby enabling proactive condition-based actions to be taken in advance [4]. For measuring distributed strain and temperature, two Brillouin-based techniques are widely used: Brillouin optical time domain reflectometry (BOTDR) based on spontaneous Brillouin scattering of a pulsed pump wave that utilizes backscattered Stokes wave; and Brillouin optical time domain analysis (BOTDA) based on stimulated Brillouin scattering that utilizes a frequency scanning counter-propagating continuous wave coupled in at another end of the same fiber against to fixed frequency pulsed pump wave. The measurand induced frequency-dependent peak (also termed as Brillouin frequency shift (BFS)) of the Brillouin gain spectrum (BGS) is linearly dependent on both strain and temperature. Standard single-mode fibers (SMF) are widely adopted for BOTDR and BOTDA systems as a fiber under test (FUT), where the measured BFS changes linearly with both strain and temperature. Unfortunately, discriminative measurement is still challenging for conventional SMF due to cross-sensitivity between strain and temperature. Thus, it is of prime importance to eliminate cross-sensitivity and accomplish true estimation of the physical measurements under interrogation.

In the literature, numerous methods have been demonstrated to show discriminative measurement of strain and temperature. A conventional method is to deploy two fibers in parallel, where one fiber is responsible for temperature sensing only while it is free from strain, whereas the other one is affected by both physical parameters. This method is expensive and requires special skills for fiber manufacturing and deployment, and complete segregation of strain and temperature is still not possible because fiber cannot be totally strain-free [5]. The other potential solution is to use double-core fiber, where each core has different strain and temperature coefficients for discriminative measurement. However, this fiber suffers cross-talk between two cores, and peak Brillouin gain levels typically are not similar, so the two cores could experience the physical parameters differently (due to the inherent non-uniformity in core cross-sections), ultimately generating large measurement errors [6–8]. Additionally, a few methods proposed are based on a combination of Rayleigh and Brillouin scattering, and Brillouin and Raman scattering, which require complex interrogation setups, thus increasing costs [9,10]. Such complex optical interrogation setups with high cost which limits the mass production and industry adoption. Discriminative measurements for short distances have also been realized using a few-mode fiber, which requires special setups for launching multiple modes in the fiber and complex detection systems [11]. Non-zero dispersion shifted fibers (DSF), such as large effective area fiber (LEAF) that have multiple acoustic modes, suggest a good candidate for multi-parameter sensing, yet these also suffer through measurement uncertainties as higher-order acoustic modes have a low level of Brillouin gain with respect to the fundamental acoustic mode, creating higher uncertainties for low BGS peaks originated from higher-order acoustic modes [12]. Various fibers that employ multiple BGS peaks for interrogation, such as inverse-parabolic graded-index fiber and orbital angular momentum guiding fiber [13], normally suffer from measurement errors due to a difference in peak gain levels (in many cases, the highest BGS peak is more than double to that of the second peak, raising diverse measurand uncertainties) as well as small differences in measurand coefficients for different peaks [14]. Therefore, it is essential to have a sensing fiber with higher BGS peaks including almost equal amplitude levels, and large differences in measurement coefficients to achieve higher accuracies.

Multi-parameter measurement errors can be minimized to the acceptance level by using a fiber that has almost the same level of peak gains, and diverse strain and temperature coefficients, such as the double-Brillouin peak fibers (DBPF) proposed in this work. The fiber is designed and fabricated with enhanced Brillouin gain response from higher-order acoustic modes so that the amplitude levels of the BGS gain peaks are at the same level. The DBPF has well-separated

Optics EXPRESS

BGS peaks in the frequency domain and peak strengths of similar amplitude levels which are well-suited for the discriminative measurements of strain and temperature. While SMF is a very suitable candidate for Brillouin sensing to quantify strain and temperature on the fiber, BFS is affected by both parameters (where lateral strain is generally neglected), axial strain, and temperature. A linear relation exists for the BFS change on temperature (ΔT) and longitudinal strain changes ($\Delta\varepsilon$):

$$\Delta\nu_{BFS} = C_T\Delta T + C_\varepsilon\Delta\varepsilon \tag{1}$$

Here, C_T and C_ε are temperature and strain sensitivities, respectively. For standard single-mode fibers, the sensitivities of temperature (C_T) and strain (C_ε) are ~1.07 MHz/°C, and ~0.046 MHz/$\mu\varepsilon$ [15,16]. Apparently, BFS is influenced by both physical parameters while interrogating for a single parameter in Brillouin sensing, thus, the measured BFS may not be accurate until proper adjustments are maintained to avoid the effect of the unwanted physical parameter. However, thanks to the continuously developing fiber manufacturing systems, fibers can be fabricated based on the requirements of specific designs. Such fibers are termed as specialty fibers, and these show a futuristic confidence for multi-parameter distributed sensing [17–20]. In short, specialty fibers offer double or multiple BGS peaks, which are advantageous to performing discriminative strain and temperature measurements using a single fiber with conventional Brillouin setups. This work demonstrates the potential of DBPF as a suitable candidate for simultaneous multi-parameter distributed sensing due to its unique enhanced double peak BGS profile. This fiber appears to be beneficial for long-distance applications such as monitoring oil and gas pipelines, bridges, and other civil infrastructures. This paper is organized as follows: Section 2 briefly describes specialty fibers and a sensing method for multi-BGS peak fibers; Section 3 includes experimental setup details, results, and discussion; and Section 4 includes conclusions and recommendations of this work.

2. Multi-peak BGS specialty fibers and sensing procedure

2.1. Suitability of the specialty fibers

Multi-Brillouin peak fibers have gained significant attention in recent years due to their unique properties and potential applications for discriminative strain and temperature sensing [21]. Previous works have studied several specialty optical fibers including polarization-maintaining fibers, dispersion compensating fibers (DCF), DSF, LEAF, photonic crystal fibers, double-clad/double-core fibers, and few-mode fibers [5,22–25]. For applications of specialty fibers in Brillouin sensing, there have been many approaches, particularly, in discriminative measurements of strain and temperature where fibers are designed to have two or multiple BGS peaks. This can be achieved by controlling the core shape, size, optical density pattern, silica material properties, and dopants (such as Ge/F); the Brillouin gain properties can be altered, thus allowing two or multiple BGS peaks [12,20,26–28]. With two or multiple BGS peaks, these fibers show potential for use in civil engineering, oil and gas, and aerospace industries to fulfill the demand for simultaneous measurements of strain and temperature with minimum errors.

The source of multiple BGSs in a single fiber can be related to the following interactions: multiple optical modes can interact with the fundamental acoustic mode; multiple acoustic modes interact with multiple/single optical modes; or multiple core fibers could generate different BFSs for each core [12]. In our work, our main focus lies on the novel DBPF, which generates two strong acoustic modes while interacting with the fundamental optical mode. Though, we also demonstrated the sensing performance of other multi-BGS fibers (LEAF in this case) with the proposed DBPF as a comparative analogy on discriminative sensing capabilities. Next, a short description is presented for these types of fibers.

LEAF: These fibers are designed for long-distance signal transmissions and have a good balance of non-linear effects and chromatic dispersion. These fibers are designed to be non-zero

Optics EXPRESS

dispersion shifted SM fibers having an effective area > 72 μm^2. A refractive index profile along the core and cladding makes these fibers special, and they are very suitable for Brillouin sensing as LEAF fibers provide multiple acoustic modes where each one resembles separate BFS in Brillouin sensing systems [12]. A primary concern lies in the strengths of the different acoustic modes, particularly, the second peak amplitude is small, which induces enormous BFS errors and also restricts long-distance sensing performances.

DBPF: This type of fiber exhibits two distinct Brillouin peaks in its Brillouin scattering spectrum. By proper designs of the core geometry and refractive index profiles, multiple acoustic modes can be achieved while maintaining single optical mode operation. Such unique BGS can be achieved by properly doping silica at the manufacturing stage with dopant materials such as germanium oxide and fluorine gas mixtures (G_eO_2 and F_2). Co-doping of these materials allows the independent control of the optical as well as acoustic index properties, and by maintaining the larger overlap between higher-order axial acoustic modes and the fundamental optical mode, peak gains in the BGS can also be increased [29–32]. A multi-step core refractive index profile allows almost equivalent peak levels in the Brillouin gain profiles achieved by doping the center region near the axis by a mixture of G_eO_2, F_2 whereas the core region near the clad interface can be doped only by G_eO_2 [32].

Let us assume a DBPF fiber with multiple BGS profile peaks, where net Brillouin gain is the sum of the contributions from all gains of the different acoustic modes.

$$G(\nu) = \sum\nolimits_m BGS_m(\nu) \tag{2}$$

Here, $BGS_m(\nu)$ is the Brillouin gain contributed by the acoustic mode m ($m = 1,\ 2$ for DPBF). at the difference frequency (between incident light frequency and stokes frequency), ν. The gain of each acoustic mode depends on the corresponding scattering cross-section (g_m), which is linearly proportional to the overlap integral between that mode's acoustic field and optical field [33].

$$BGS_m(\nu) = g_m^2 \frac{\left(\frac{\Delta\nu_B}{2}\right)^2}{\left[(\nu - \nu_{B,m})^2 + \left(\frac{\Delta\nu_B}{2}\right)^2\right]} \tag{3}$$

$$g_m \propto \frac{\left(\int E_o E_o^* \rho_a r dr d\theta\right)^2}{\int (E_o E_o^*)^2 r dr d\theta \int \rho_a \rho_a^* r dr d\theta} \tag{4}$$

where $\Delta\nu_B$ is the BGS linewidth measured at full width at half maximum (FWHM), $\nu_{B,m}$ is the optical frequency shift of the backscattered stokes light from initial light corresponding to mode peak gain, E_o and ρ_a are scalar field amplitudes of the optical and acoustic fields and are functions of the cylindrical coordinate parameters r and θ, which are radial distance and azimuthal angle respectively. The overlap integral is zero for the non-axial acoustic modes. The required acoustic and optical fields are calculated by solving the scalar wave equations (assuming weakly guided approximation) [29,30,33].

$$\frac{d^2E_o}{dr^2} + \frac{1}{r}\frac{dE_o}{dr} + k_o^2\left[n_o^2(r) - n_{O_{eff}}^2(r)\right]E_o = 0 \tag{5}$$

$$\frac{d^2\rho_a}{dr^2} + \frac{1}{r}\frac{d\rho_a}{dr} + \frac{k_a^2}{C}\left[n_a^2(r) - n_{a_{eff}}^2(r)\right]\rho_a = 0 \tag{6}$$

In the equations above, k_o is the optical wave number, λ is the peak optical wavelength, $n_o(r)$ is the fiber refractive index, whereas $n_{o_{eff}}(r)$ is the effective refractive index of the optical fundamental mode, k_a. is the acoustic wave number, $k_a = 2k_o n_{o_{eff}}$ is used to satisfy the phase-matching condition between acoustic and optical fields. Furthermore, $n_a(r)$ is the longitudinal

Optics EXPRESS

acoustic refractive index, $n_{a_{eff}}(r)$ is the effective longitudinal refractive index of the acoustic modes, $n_{e_{eff}}(r)$ is the effective longitudinal refractive index of the acoustic mode, and C is a constant. The BFS can then be lculated as: $\nu_{BFS} = 2.\frac{V_{clad}}{\lambda}.\ \frac{n_{o_{eff}}}{n_{a_{eff}}}$, where V_{clad} is the longitudinal acoustic velocity in silica cladding. Clearly, by managing effective index parameters in the geometrically designed fiber core, we can achieve double peaks in the BGS. The simulated BGS profile as a function of Brillion frequency (frequency difference between pump wave and probe wave) at a 1550 nm pump wavelength for DBPF is illustrated in Fig. 1.

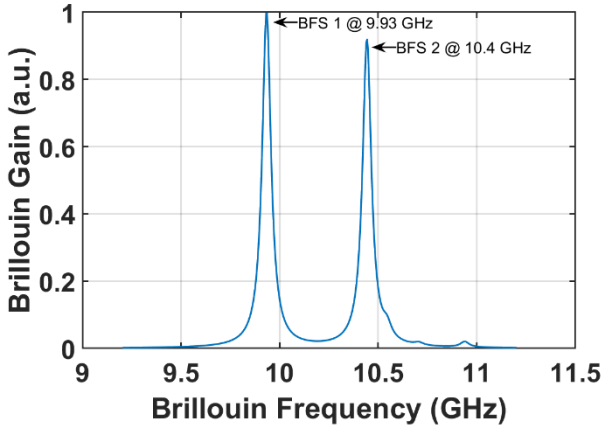

Fig. 1. Simulated Brillouin gain profile in DBPF: two BFSs separated by 510 MHz, and the second peak level lies within 10% of that of the first peak. The frequency position of these peaks depends on both strain and temperature through the dependence of the local acoustic velocities, v_a, on these two measurands.

2.2. *Discriminative strain and temperature sensing of multi-peak BGS fibers*

The use of discriminative Brillouin sensing allows for more accurate and precise measurement of physical quantities (strain and temperatures), as compared to a general-purpose sensor which mainly relies on the single BGS peak of silica SMF. High accuracy and simultaneous measurements require distinctive intense BGS peaks with differences in sensitivity coefficients. As the difference in the measurand coefficients increases between the two peaks, cross measurand influence can be reduced. The strain and temperature evaluations in a single fiber at the same time can be accomplished using the following relation [34,35]:

$$\begin{bmatrix} \Delta\nu_{BFS1} \\ \Delta\nu_{BFS2} \end{bmatrix} = \begin{bmatrix} C_{T1} & C_{\varepsilon 1} \\ C_{T2} & C_{\varepsilon 2} \end{bmatrix} \begin{bmatrix} \Delta T \\ \Delta\varepsilon \end{bmatrix}; \text{ or } [\nu] = [C]\ [M], \text{ or } [M] = [A]^{-1}[\nu] \qquad (7)$$

The terms C_{T1}, $C_{\varepsilon 1}$ in the matrix C are sensitivity coefficients for temperature and strain for BGS peak 1 (ν_{BFS1}), whereas C_{T2}, $C_{\varepsilon 2}$ belong to BGS peak 2 (ν_{BFS2}). Once we identify the sensitivity coefficient matrix, we can use it in Eq. (7) to obtain the measurand values by simply solving the inverse matrix problem. The coefficients matrix represents the slope parameter of the BFS vs. msurand curves for each acoustic mode. The coefficient matrix can be calculated by performing BFS measurements by changing one parameter only and keeping the other fixed for each measurement. Thus, once the coefficient matrix is obtained, simultaneous experiments to measure strain and temperature can be performed. The measurement error in the quantification of both parameters will depend on the possible errors of the BFS ($\delta\nu_B{}^1$ *and* $\delta\nu_B{}^2$) from the

Optics EXPRESS

measurements. Once, BFS errors for each BGS peak are calculated, we can use the following relation to calculate temperature (δT) and strain errors ($\delta\varepsilon$) [20].

$$\delta T = \frac{|C_\varepsilon^2|\delta\nu_B{}^1 + |C_\varepsilon^1|\delta\nu_B{}^2}{|C_\varepsilon^2 C_T^1 - C_\varepsilon^1 C_T^2|} \quad ; \quad \delta\varepsilon = \frac{|C_T^2|\delta\nu_B{}^1 + |C_T^1|\delta\nu_B{}^2}{|C_\varepsilon^2 C_T^1 - C_\varepsilon^1 C_T^2|} \tag{8}$$

3. Experimental setup, results, and discussions

The BOTDA system schematic representation shown in Fig. 2 demonstrates the capability of simultaneous and discriminative strain and temperature sensing. A distributed-feedback (DFB) laser at 1550 nm wavelength was used as an optical source and split into two propagation paths using a 50/50 3 dB fiber coupler. A polarization controller (PC) was employed at the input of each Mach-Zehnder modulator (MZM) for obtaining the maximum optical power at the output. MZM 1 modulates the input signal at a frequency of sensing fiber BFS in a carrier suppression mode, which is driven by an external tunable frequency synthesizer. An MZM 2 modulates the electrical pulses into optical pulses using a pulse generator at a desired pulse width, peak-to-peak amplitude, and repetition rate. Afterward, the continuous wave probe and pump pulse signals are amplified by an erbium-doped fiber amplifier (EDFA). Two bandpass filters were used after each EDFA to eliminate amplified spontaneous emission (ASE) noise. Adjusting the operating current of the EDFAs, the pump and probe powers are separately optimized at the sensing fiber input. A polarization scrambler (PS) is used to eliminate the polarization-induced fluctuations in measured Brillouin spectra. The Brillouin signal is then collected by a circulator port 3, then detected by a photodetector, and analyzed using an oscilloscope at a sampling rate of 1 GS/s. The fiber under test consists of standard SMF, DBPF, and LEAF fibers.

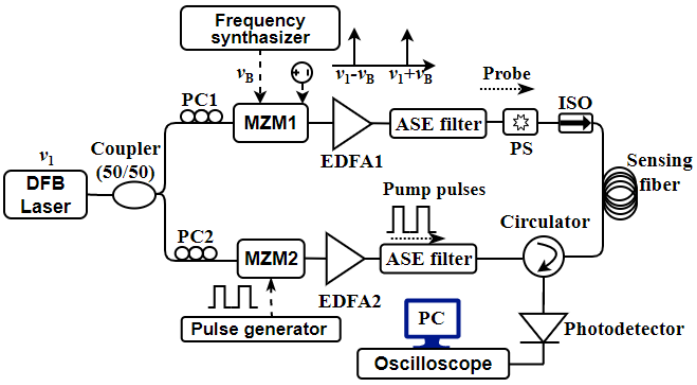

Fig. 2. Schematic setup of BOTDA system.

Initially, we measured a BFS for each sensing fiber, and their three-dimensional (3D) spectral mapping was obtained by sweeping the synthesizer frequencies around the BFS with a frequency step of 2 MHz and 2,000 trace averages. Using a multi-peak Lorentz curve fitting to the measured raw BGS data over the sensing fiber distance, the BFS distribution was obtained for all types of sensing fibers (SMF, DBPF, and LEAF fibers).

3.1. Evaluation of the BGSs, BFS uncertainty, and measurement coefficients

We measured the BGSs individually for each sensing fiber of DBPF, LEAF, and standard SMF, as illustrated in Fig. 3. For a fair comparison, we extracted the BGSs of all three fibers at the same location of 100 m distance. From Fig. 3, besides the fundamental Brillouin peak at 9.885 GHz, the higher-order Brillouin peaks at 10.39 GHz are clearly noticeable in DBPF (named as peak 1 and

Optics EXPRESS

peak 2) with enhanced Brillouin gain and large frequency separation between them. The LEAF exhibits three BGS peaks corresponding to three acoustic modes, caused by a triangle refractive index profile. For Brillouin sensors employing multi-Brillouin peak fibers, it is ideal to have enhanced gain response with equal amplitude levels to reduce the BFS uncertainties, since the low Brillouin gain peak gives rise to larger BFS errors. On the other hand, the smaller frequency separation between the Brillouin peaks limits the maximum strain/temperature measurements and ideally requires large frequency separation to avoid overlapping between these two BGS peaks. From Fig. 3 and Table 1, it is obvious that the DBPF exhibits a lower amplitude difference of just 0.4 dB between its two peaks, while contrary to it, that of LEAF lies at 4.7 dB between the two highest peaks, and the frequency separation between the two Brillouin peaks is 505 MHz for DBPF (which is close to the simulated BGS profile frequency separation of ~510 MHz shown in Fig. 1) and 210 MHz for LEAF. It is evident that the DBPF is most suitable for discriminative strain and temperature sensing with enhanced performance.

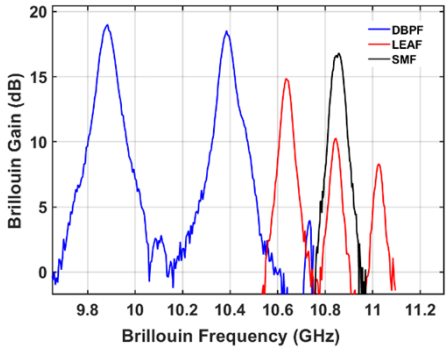

Fig. 3. The measured Brillouin gain spectrums of DBPF, LEAF, and standard SMF.

Table 1. Comparison of BGS Parameters for Different Fiber Types

Fiber Type	Peak Amplitude (Peak 1, 2) in dB	Frequency (MHz), and Amplitude (dB) difference (Peak 1, 2)
SMF	16.8, NA	NA
LEAF	14.86, 10.18	Freq: 210 Ampl: 4.7
DBPF	**19, 18.53**	**Freq: 505** **Ampl: 0.47**

Firstly, we demonstrated a LEAF fiber's sensing performance and also calculated its BFS uncertainties (estimated BFS errors) over the fiber distance. Figure 4(a). shows a 3D spectrum over a 25 km long LEAF and has distinct Brillouin peaks originated by multiple acoustic modes and separated by their distinct BGS (here, the adjacent BFS separation > 200 MHz) peak values.

As described previously, the first peak's Brillouin gain level appears to be stronger than the second and third peaks by three and four times, respectively. This difference in peak gain causes different levels of signal-to-noise ratio (SNR) associated with different acoustic modes, which ultimately results in more error in temperature/strain measurements, and larger BFS uncertainties corresponding to higher-order acoustic modes. As shown in Fig. 4(b), all three peaks shift linearly with temperature variations up to 90 °C. In order to measure the BFS uncertainty over the fiber distance, we adopted a well validated method proposed by M. Soto *et al.* [36], which is based on the parameters of frequency scanning step, Brillouin gain linewidth at FWHM and signal-to-noise

Optics EXPRESS

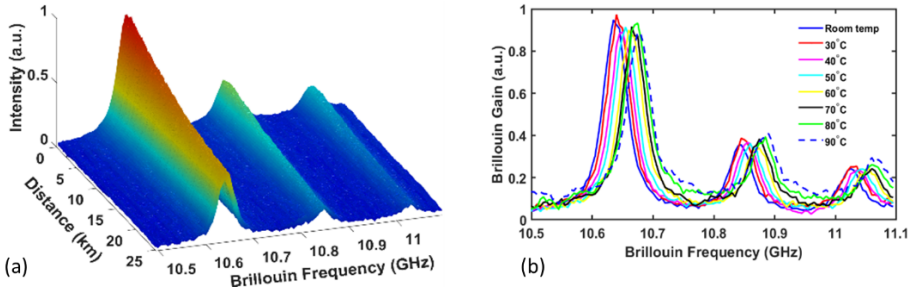

Fig. 4. (a): 3D BGS of LEAF fiber at room temperature along the 25-km length fiber; where the first BGS peak has a larger amplitude level corresponding to the second and third ones, (b): BGS profile at the sensing fiber end for various temperatures ranging from ambient room temperature to 90 °C.

ratio of the signal trace at peak gain. Figure 5. (a) shows measured BFS uncertainties along the LEAF. The estimated BFS error at the fiber end was found to be as high as 0.18 MHz for peak 1, and 0.42 MHz for peak 2, translating it to unsuitable for discriminative sensing in longer-distance monitoring. It shows that as the peak level in higher acoustic modes decreases along the length, measurement errors arise.

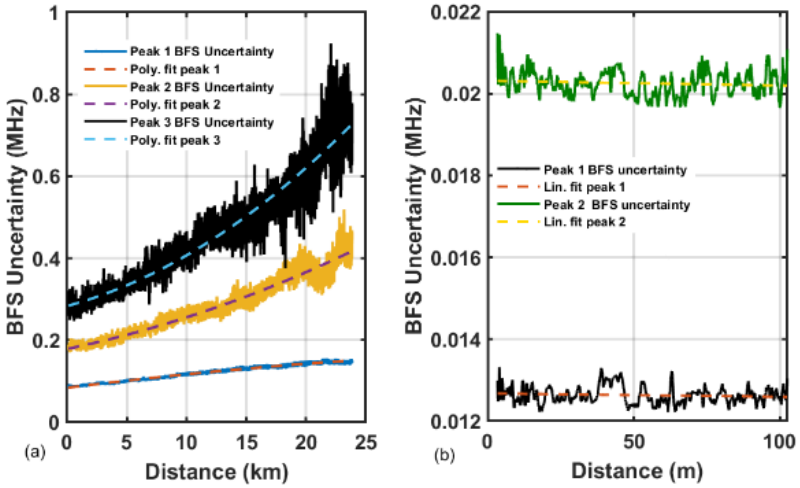

Fig. 5. Calculated BFS uncertainty over the fiber distance (a) LEAF and (b) DBPF fiber. (Here the BFS uncertainty is calculated as a function of BGS linewidth, SNR of the trace at the peak gain, frequency scanning step of the probe wave, and a fraction of peak gain level for selecting frequency points for quadratic fitting [36].)

DBPF fiber of 100-m length was then interrogated. Figure 6 shows Brillouin gain profiles, which clearly indicate: (i) both BGS peaks and linewidth are of comparable levels (the second peak is smaller than the first peak by less than 10% of the first peak), which helps to maintain sensitivity coefficients as well as BFS measurements with minimum and almost similar level errors in both modes; and (ii) two peaks are well separated, allowing large amplitude variations for any measurands. We also plotted BFS uncertainty for DBPF along the fiber (Fig. 5(b)) and observed that this fiber is more resistant to noise, thereby enhancing measurement accuracy. The DBPF fiber shows negligible uncertainty in both peaks, estimated BFS errors of 0.01 MHz for peak 1, and 0.02 MHz for peak 2. Observing the pattern of BFS uncertainties in both peaks, it is

Optics EXPRESS

clear that uncertainty will not grow adversely even for longer lengths. Furthermore, to have a fair comparison between LEAF and DBPF, we analyzed the BFS uncertainty of LEAF for the first 100 m, which shows estimated BFS error of its highest peak is five and ten times larger than that of peak 1 and peak 2 of the DBPF, whereas the second and third peaks of LEAF are even worse.

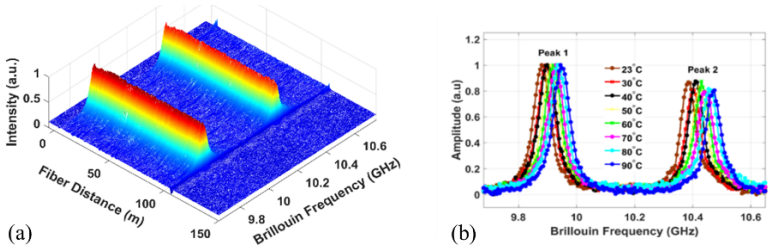

Fig. 6. (a): DBPF fiber's 3D BGS at ambient room temperature, peak gain values for two acoustic modes are of similar strengths (<10% difference in their levels), and well separated in frequency > 500 MHz, (b): BGSs obtained at the end of the 100 m fiber, where BFS-peak 1 and BFS-peak 2 respond linearly with the temperature variations.

The evaluation of the strain and temperature coefficients for each fiber type was performed by varying one parameter precisely while keeping the other parameter fixed for each measurement, and vice versa. To create strain/temperature variations, the two FUT sections were kept apart by a few tens of meters. We carried out independent measurements of temperatures up to 95 °C. (at constant strain condition) and strains up to 2,040 micro strains (at constant temperature). The resulting sensitivity curves of the strain and temperature for the DBPF fibers are plotted in Fig. 7. For other types of fibers, a summary of the parameters is available in Table 2.

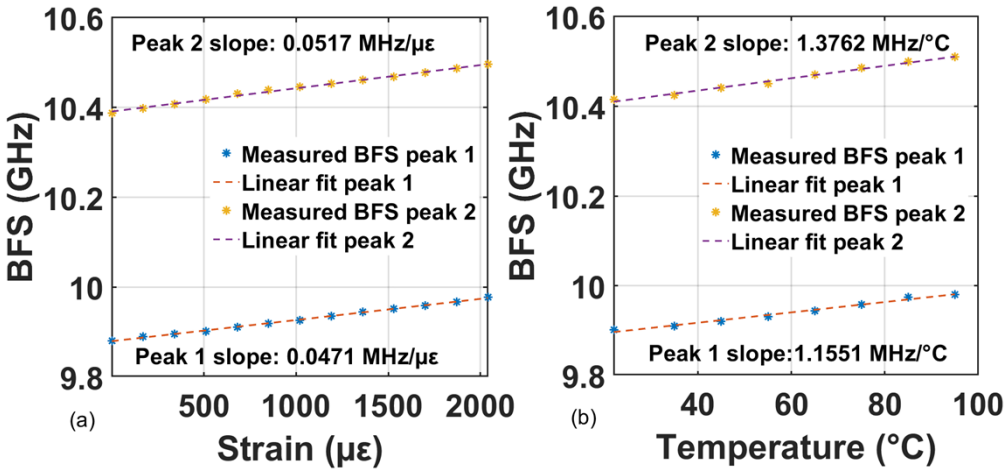

Fig. 7. (a): BFS curve at the center of the FUT for strain variations, the obtained sensitivities of two acoustic modes appear to be distinct; (b): BFS curves for temperature variations. With linear fitting to the BFS data to the measurand variations, coefficients of strains/temperature for each peak are calculated as slopes.

Optics EXPRESS

Table 2. Comparison of BGS Profiles and Relative Analysis for Different Fiber Types

Fiber Type	Peak BFS (GHz)		Temperature Coefficient (MHz/°C)	Strain Coefficient (MHz/με)	BFS Uncertainty (estimated BFS error) at 100 m Distance (MHz)
SMF	10.84		1.033	0.0499	0.04300
LEAF	Peak 1	10.64	1.018	0.0377	0.0900
	Peak 2	10.85	0.918	0.0374	0.1870
DBPF (this work)	**Peak 1**	**9.885**	**1.1551**	**0.0471**	**0.0129**
	Peak 2	**10.39**	**1.3762**	**0.0517**	**0.0217**

The obtained sensitivity matrix is given where temperature coefficients are well separated by > 0.2 MHz/°C, which is an exciting indication for discriminative sensing.

$$S_{\mathrm{DBPF}} = \begin{bmatrix} 1.1551 & 0.0471 \\ 1.3762 & 0.0517 \end{bmatrix} \tag{9}$$

The gain spectrum analysis for the different types of fibers is summarized in Table 2. The major source of measurement error arises due to differences of peak gain levels in BGS originated by different acoustic modes; BFS errors rise for higher-order peaks. LEAF BGS have higher-order peaks with lower strengths and suffer more measurement errors in comparison to DBPF, which have enhanced pes. Clearly, these results show the benefits of using DBPF fiber for long-distance distri.uted structure health monitoring. The BFS uncertainty for different fibers at the same length position under similar experimental parameters shows DBPF has superior performance.

3.2. *Simultaneous measurements of strain and temperature*

To verify the DBPF's simultaneous measurement capability, an experiment was carried out by applying strain and temperature variations simultaneously in the same fiber section. A fiber of 1-m length was fixed between two ends, with controlled heating and strain variation arrangements. The baseline measurement was taken keeping the strained fiber at 22 °C, then, for the simultaneous measurement, the fiber was strained by 1220 $\mu\varepsilon$ and the temperature was increased to 62 °C.

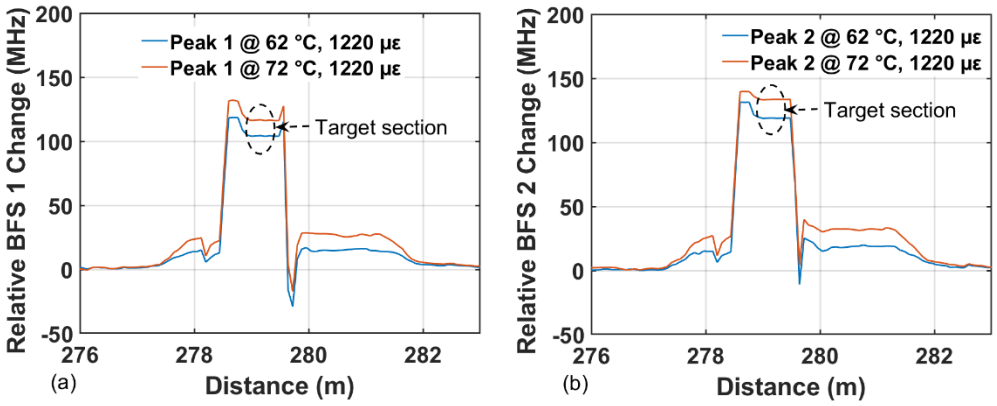

Fig. 8. (a): BFS curves (relative to baseline) for peak 1 at different temperature/strain variations, (b): BFS curves (relative to baseline) for peak 2. The expected section for analyzing simultaneous measurement is center of the FUT, interrogated by 50 cm resolution BOTDA.

Optics EXPRESS

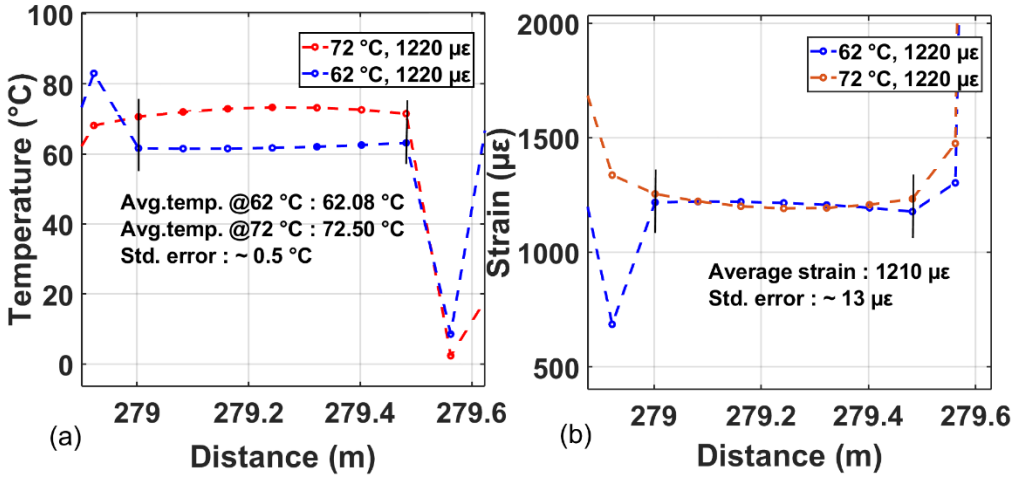

Fig. 9. Simultaneously measured temperature (a) and strain (b) in DBPF fibers using BOTDA.

Next, the temperature was further increased to 72 °C by keeping the same level of strain (1220 $\mu\varepsilon$).

Considering the central section of the FUT (the dotted target section in Fig. 8.), maximum BFS error was evaluated to be equal to ~0.18 MHz for each peak, which is due to different experimental conditions (spatial resolution, number of averages, SNR, control the BFS uncertainties) in comparison to the condition while evaluating coefficients. The corresponding strain and temperature standard deviation errors were then calculated from the measured strain and temperature values and obtained as ±13 $\mu\varepsilon$, and ±0.5 °C. It is important to mention that due to limitation of simultaneous experimental adjustments, we only consider the central half section of the FUT (central section length <1 m) for discriminative measurements. As shown in Fig. 9, we can see that the results match as desired: the strain is the same ~ 1210 $\mu\varepsilon$ for two temperature conditions, whereas temperatures are 62.08 °C and 72.50 °C, as expected.

4. Conclusion

We have analyzed the DBPF's discriminative sensing capabilities and experimentally demonstrated its superior performance. Compared to the other multi-BGS fibers, such as LEAF, DBPF exhibits one fifth the BFS uncertainty of LEAF under similar conditions. Fibers such as LEAF and DCF, despite having multiple peaks in their gain profiles, are dominated by large measurement errors. This is primarily attributed to the dominance of a higher order acoustic mode contributing lesser peak gain than two times that of the highest gain peak associated to fundamental acoustic mode. For long-distance monitoring, it is important to have high SNR for the different gain peaks, and therefore LEAF and DCF fibers are inefficient for long-distance sensing. SSMF can only be used in single parameter monitoring and is always affected by cross-sensitivity issues. However, the DBPF possesses clearly comparable levels of gains, well separated gain peaks in frequency domain, and distinct values of strain and temperature coefficients associated to two acoustic modes. As we have shown experimentally, the maximum strain and temperature measurement error obtained were ±13 $\mu\varepsilon$ and ±0.5°C, respectively. It was validated that DBPF is free of cross-sensitivity issues, and high-accuracy strain and temperature measurements can be performed simultaneously. We believe that with better experimental conditions we can further minimize these errors, since temperature coefficients are separated by >0.2 MHz/°C, suitable for discriminatory measurements. The DBPF fiber can have a significant role as sensing

Optics EXPRESS

materials where require multi-parameter sensing capabilities such as monitoring of natural gas infrastructures up to tens of kilometers.

Funding. U.S. Department of Energy.

Acknowledgements. This work was performed in support of the U.S. Department of Energy's (DOE) Fossil Energy and Carbon Management and executed through the National Energy Technology Laboratory (NETL) Research & Innovation Center's Natural Gas Infrastructure FWP.

Disclosures. The authors declare no conflict of interest.

Data Availability. The datasets generated during the current study are available from the corresponding author on reasonable request and need.

References

1. A. Güemes and J. M. Menendez, "Fiber-Optic Sensors," in *Structural Health Monitoring*, ed: Wiley, 2006, pp. 225–285.
2. D. A. Krohn, T. MacDougall, and A. Mendez, *Fiber optic sensors: fundamentals and applications*: Spie Press Bellingham, WA, 2014.
3. M. A. Soto, G. Bolognini, and F. Di Pasquale, "Optimization of long-range BOTDA sensors with high resolution using first-order bi-directional Raman amplification," Opt. Express **19**(5), 4444–4457 (2011).
4. R. Di Sante, "Fibre optic sensors for structural health monitoring of aircraft composite structures: Recent advances and applications," Sensors **15**(8), 18666–18713 (2015).
5. X. Bao, D. J. Webb, and D. A. Jackson, "Combined distributed temperature and strain sensor based on Brillouin loss in an optical fiber," Opt. Lett. **19**(2), 141–143 (1994).
6. M.-J. Li, S. Li, and J. A. Derick, *et al.*, "Dual core optical fiber for distributed Brillouin fiber sensors," in *Asia Communications and Photonics Conference*, 2014, p. AW4I. 3.
7. Y. Mizuno, N. Hayashi, H. Tanaka, Y. Wada, and K. Nakamura, "Brillouin scattering in multi-core optical fibers for sensing applications," Sci. Rep. **5**(1), 11388 (2015).
8. Z. Zhao, Y. Dang, and M. Tang, *et al.*, "Spatial-division multiplexed Brillouin distributed sensing based on a heterogeneous multicore fiber," Opt. Lett. **42**(1), 171–174 (2017).
9. D.-P. Zhou, W. Li, L. Chen, and X. Bao, "Distributed temperature and strain discrimination with stimulated Brillouin scattering and Rayleigh backscatter in an optical fiber," Sensors **13**(2), 1836–1845 (2013).
10. Y. Muanenda, C. J. Oton, and F. Di Pasquale, "Application of Raman and Brillouin scattering phenomena in distributed optical fiber sensing," Front. Phys. **7**, 155 (2019).
11. A. Li, Y. Wang, J. Fang, M.-J. Li, B. Y. Kim, and W. Shieh, "Few-mode fiber multi-parameter sensor with distributed temperature and strain discrimination," Opt. Lett. **40**(7), 1488–1491 (2015).
12. X. Liu and X. Bao, "Brillouin spectrum in LEAF and simultaneous temperature and strain measurement," J. Lightwave Technol. **30**(8), 1053–1059 (2012).
13. L. Sheng, L. Huang, and J. Yan, *et al.*, "Distributed multi-parameter sensing based on the Brillouin scattering effect in orbital angular momentum guiding fiber," Opt. Continuum. **1**(1), 133–142 (2022).
14. Y. Xu, M. Ren, and Y. Lu, *et al.*, "Multi-parameter sensor based on stimulated Brillouin scattering in inverse-parabolic graded-index fiber," Opt. Lett. **41**(6), 1138–1141 (2016).
15. X. Bao and L. Chen, "Recent progress in distributed fiber optic sensors," Sensors **12**(7), 8601–8639 (2012).
16. A. H. Hartog, *An introduction to distributed optical fibre sensors*: CRC press, 2017.
17. P. Dragic and J. Ballato, "A brief review of specialty optical fibers for Brillouin-scattering-based distributed sensors," Appl. Sci. **8**(10), 1996 (2018).
18. Y. Sun, H. Li, and C. Fan, *et al.*, "Review of a specialty fiber for distributed acoustic sensing technology," in *Photonics*, 2022, p. 277.
19. T. Weijun, Y. Chen, and L. Tongqing, *et al.*, "Progress and prospect of novel specialty fibers for fiber optic sensing," Opt. Electron. Eng. **45**(9), 180243 (2018).
20. X. Sun, K. Bedard, M. Hines, J. Li, and R. Dyer, "Simultaneous distributed strain and temperature measurement using a dual-Brillouin-peak optical fiber," in *Fiber Optic Sensors and Applications XVI*, 2019, 20–24.
21. A. Othonos, K. Kalli, D. Pureur, and A. Mugnier, *Fibre bragg gratings*: Springer, 2006.
22. C. Lee, P. Chiang, and S. Chi, "Utilization of a dispersion-shifted fiber for simultaneous measurement of distributed strain and temperature through Brillouin frequency shift," IEEE Photonics Technol. Lett. **13**(10), 1094–1096 (2001).

Optics EXPRESS

23. Z. Li, L. Yan, X. Zhang, and W. Pan, "Temperature and strain discrimination in BOTDA fiber sensor by utilizing dispersion compensating fiber," IEEE Sens. J. **18**(17), 7100–7105 (2018).
24. J. E. McElhenny, R. Pattnaik, and J. Toulouse, "Polarization dependence of stimulated Brillouin scattering in small-core photonic crystal fibers," J. Opt. Soc. Am. B **25**(12), 2107–2115 (2008).
25. L. Zou, X. Bao, S. Afshar, and L. Chen, "Dependence of the Brillouin frequency shift on strain and temperature in a photonic crystal fiber," Opt. Lett. **29**(13), 1485–1487 (2004).
26. X. Bao, Z. Zhou, and Y. Wang, "distributed time-domain sensors based on Brillouin scattering and FWM enhanced SBS for temperature, strain and acoustic wave detection," PhotoniX **2**(1), 14–29 (2021).
27. Y. Dong, L. Chen, and X. Bao, "High-spatial-resolution time-domain simultaneous strain and temperature sensor using Brillouin scattering and birefringence in a polarization-maintaining fiber," IEEE Photonics Technol. Lett. **22**(18), 1364–1366 (2010).
28. M. A. Zaghloul, M. Wang, and G. Milione, *et al.*, "Discrimination of temperature and strain in Brillouin optical time domain analysis using a multicore optical fiber," Sensors **18**(4), 1176 (2018).
29. M.-J. Li, X. Chen, and J. Wang, *et al.*, "Al/Ge co-doped large mode area fiber with high SBS threshold," Opt. Express **15**(13), 8290–8299 (2007).
30. M. Mermelstein, M. Andrejco, and J. Fini, *et al.*, "11.2 dB SBS gain suppression in a large mode area Yb-doped optical fiber," in *Fiber Lasers V: Technology, Systems, and Applications*, 2008, 97–103.
31. K. Y. Song, M. G. Herráez, and L. Thévenaz, "Gain-assisted pulse advancement using single and double Brillouin gain peaks in optical fibers," Opt. Express **13**(24), 9758–9765 (2005).
32. X. Sun, K. Bedard, J. Li, and R. S. Dyer, "A dual-Brillouin-peak optical fiber for simultaneous distributed strain and temperature measurement," in *Advanced Sensor Systems and Applications VIII*, 2018, 7–12.
33. A. Yeniay, J.-M. Delavaux, and J. Toulouse, "Spontaneous and stimulated Brillouin scattering gain spectra in optical fibers," J. Lightwave Technol. **20**(8), 1425–1432 (2002).
34. M. Davis and A. Kersey, "Simultaneous measurement of temperature and strain using fibre Bragg gratings and Brillouin scattering," IEE Proc., Optoelectron. **144**(3), 151–155 (1997).
35. D. J. J. Hu, G. Humbert, H. Dong, H. Zhang, J. Hao, and Q. Sun, "Review of specialty fiber based Brillouin optical time domain analysis technology," in *Photonics*, 2021, p. 421.
36. M. A. Soto and L. Thévenaz, "Modeling and evaluating the performance of Brillouin distributed optical fiber sensors," Opt. Express **21**(25), 31347–31366 (2013).